Counteracting Rapid Catalyst Deactivation by Concomitant Temperature Increase during Catalytic Upgrading of Biomass Pyrolysis Vapors Using Solid Acid Catalysts

Andreas Eschenbacher [1] , **Alireza Saraeian** [2], **Brent H. Shanks** [2], **Uffe Vie Mentzel** [3] ,
Jesper Ahrenfeldt [1], **Ulrik Birk Henriksen** [1] **and Anker Degn Jensen** [1,*]

1   Department of Chemical and Biochemical Engineering, Technical University of Denmark, 2800 Kgs. Lyngby,
    Denmark; aesc@kt.dtu.dk (A.E.); jeah@kt.dtu.dk (J.A.); ubhe@kt.dtu.dk (U.B.H.)
2   Department of Chemical and Biological Engineering, Iowa State University, Ames, IA 50011, USA;
    alirezas@iastate.edu (A.S.); bshanks@iastate.edu (B.H.S.)
3   Haldor Topsøe A/S, 2800 Kgs. Lyngby, Denmark; UFVM@topsoe.com
*   Correspondence: aj@kt.dtu.dk; Tel.: +45-45-25-28-41

Abstract: The treatment of biomass-derived fast pyrolysis vapors with solid acid catalysts (in particular HZSM-5 zeolite) improves the quality of liquid bio-oils. However, due to the highly reactive nature of the oxygenates, the catalysts deactivate rapidly due to coking. Within this study, the deactivation and product yields using steam-treated phosphorus-modified HZSM-5/γ-Al$_2$O$_3$ and bare γ-Al$_2$O$_3$ was studied with analytical Py-GC. While at a fixed catalyst temperature of 450 °C, a rapid breakthrough of oxygenates was observed with increased biomass feeding, this breakthrough was delayed and slower at higher catalyst temperatures (600 °C). Nevertheless, at all (constant) temperatures, there was a continuous decrease in the yield of oxygen-free hydrocarbons with increased biomass feeding. Raising the reaction temperature during the vapor treatment could successfully compensate for the loss in activity and allowed a more stable production of oxygen-free hydrocarbons. Since more biomass could be fed over the same amount of catalyst while maintaining good deoxygenation performance, this strategy reduces the frequency of regeneration in parallel fixed bed applications and provides a more stable product yield. The approach appears particularly interesting for catalysts that are robust under hydrothermal conditions and warrants further investigations at larger scales for the collection and analysis of liquid bio-oil.

Keywords: phosphorus; HZSM-5; γ-Al$_2$O$_3$; biomass; catalytic fast pyrolysis; catalyst activity

1. Introduction

Bio-oils obtained from the fast pyrolysis (FP) of biomass differ from conventional petroleum-derived fuels and require significant upgrading before they can be used as transportation fuels. The challenges of upgrading biomass-derived fast pyrolysis oils have been reviewed recently [1–4]. The deoxygenation of biomass-derived fast pyrolysis vapors can be achieved by using solid acid or base catalysts in the temperature range of ~400–600 °C [5–14]. Zeolite-based catalysts represent the current state of the art [15–17] and favor dehydration, decarbonylation, cracking, and aromatization reactions [18,19]. Strong acid sites and shape-selective pores of the medium pore size HZSM-5 yield high-value monoaromatics (benzene, toluene, ethylbenzene, and xylene), propylene, and lower coke yields compared to other zeolites or solid acid catalysts [15,20]. In addition, aromatic formation results from Diels-Alder reactions between alkenes and biomass-derived furans [21]. Higher catalyst

temperatures favor gas formation due to cracking reactions [22], and for HZSM-5 catalysts, increased yields of alkenes and aromatics are often observed at ~600 °C [23–25]. Patel et al. [22] reported that the amount of aliphatic and aromatic -OH groups decreased as the upgrading temperature was increased from 500 to 550 °C using HZSM-5 as a catalyst, but there was less impact when the temperature was further increased to 600 °C. Due to the hydrogen-deficient nature of biomass, a high degree of oxygen removal can only be achieved by severely decreasing the yield of bio-oil due to the carbon losses to light gases and coke. The challenge is, therefore, to improve the yields of stabilized liquid bio-oil without the introduction of costly hydrogen [17,26].

In the present work, the focus lies on upgrading biomass-derived fast pyrolysis vapors outside the pyrolysis reactor in a close-coupled catalyst reactor prior to vapor condensation (often termed ex situ catalytic fast pyrolysis). This process configuration can prevent the poisoning of catalytic active sites due to ash species [27–29] and allows for the independent temperature control of the pyrolysis and catalytic reactor. Using HZSM-5 as a catalyst, the selectivity of oxygen-free hydrocarbons (HCs) is highest in the initial upgrading phase over a fresh catalyst (at high rates of coke and light gas formation from cracking reactions and thus low organic liquid yield), and then gradually deteriorates due to the incomplete conversion of oxygenates. The rate and extent of the deactivation of the catalyst by coking is therefore a major issue for its industrial implementation in this application [27,30]. Diebold and Scahill [31] already pointed out over three decades ago that a catalytic reactor, which can maintain a high level of catalytic activity in spite of high coking rates, would be desired. The coking problem with zeolites can in principle be addressed by a conventional fluidized catalytic cracking (FCC) arrangement with continuous catalyst regeneration by the oxidation of the coke. However, significant carbon losses to coke and gas occur at the initial upgrading period over a freshly regenerated catalyst [27]. The initially high rate of coke deposition is followed by a much lower rate of coke deposition [30,32–35]. Based on this, regenerating the catalyst incompletely, in order to reduce the initial carbon losses to coke and benefit from a lower coking rate compared to upgrading over a fresh catalyst, was suggested [32]. However, a not fully regenerated catalyst will have a lower time on stream before regeneration is required again. As pointed out recently by Perkins et al. [36], the economic conversion of biomass feedstocks into partially upgraded bio-crudes may require novel reactor concepts. Under the commercial operating conditions of catalytic reforming, hydrotreating, hydrocracking, and such processes, the temperature of the catalyst bed is raised gradually to compensate for the loss in activity [37,38]. However, in these processes, the coke accumulates on the catalyst very slowly over the course of several months. In the present work, the concept of a dynamic temperature increase in the catalytic reactor was investigated in order to counteract initial low liquid yields and the rapid catalyst deactivation during biomass feeding. To the best of our knowledge, this approach has not been tested for the catalytic treatment of fast pyrolysis vapors.

Specifically, we investigated if starting the upgrading of biomass-derived pyrolysis vapors at a low catalyst temperature of 450 °C, and increasing the catalyst temperature during the upgrading, can compensate for the loss in catalyst activity due to the rapid coking, thereby allowing the feeding of more biomass over a fixed amount of catalyst before regeneration is required. In addition, it was of interest to investigate if, for a certain degree of vapor deoxygenation, the dynamic temperature approach may allow the limitation of the carbon losses to coke, CO, and CO_2 compared to operating at a constant catalyst temperature.

The performance of a steam-treated HZSM-5/γ-Al$_2$O$_3$ extrudate as a catalyst for the deoxygenation of wheat straw fast pyrolysis vapors has been reported previously [28,39]. For the present work, HZSM-5/γ-Al$_2$O$_3$ extrudates were modified with 0.5 wt% phosphorus in order to improve the hydrothermal stability of the HZSM-5 component, as reported in several studies [40–46]. Cerqueira et al. [47] noted that before the steam treatment, impregnation with phosphorus produces several counterproductive effects: (i) a reversible decrease in activity due to the interaction of P species with the protonic sites; (ii) external surface blockage; (iii) a decrease in the microporous volume; and even (iv) dealumination. Nevertheless, during steam exposure, the phosphorus-impregnated samples

retained their acidity and activity at a higher level compared to the untreated zeolite. This indicates that the introduction of phosphorus can reinforce the zeolite structure and prevent dealumination [48,49], with the stabilization effect being more evident in more severe treatment conditions [43].

Besides using P-modified HZSM-5/γ-Al$_2$O$_3$ as catalyst, the present work also investigated using γ-Al$_2$O$_3$ for vapor deoxygenation as a low-cost and hydrothermally stable alternative to zeolite-containing catalysts.

2. Results

2.1. Catalyst Properties

The physicochemical properties of γ-Al$_2$O$_3$ and HZSM-5/γ-Al$_2$O$_3$ extrudates were detailed in previous work [28]. Table 1 provides an overview of the textural properties and the acidity of the different catalysts (steamed) that were tested in the present work. The pore size distribution of the micropores, obtained by applying the non local density functional theory (NLDFT) model to the adsorption branch of the isotherms, obtained from argon physisorption at 87 K, is shown in Figure S1a. The size distribution of mesopores, obtained by applying the Barrett, Joyner, and Halenda (BJH) model to the adsorption branch of the nitrogen physisorption (77 K) isotherms, is shown in Figure S1b. γ-Al$_2$O$_3$ is purely mesoporous. The slightly higher mesoporous volume compared to the total pore volume (directly determined from adsorption data) for Al$_2$O$_3$ is attributed to the uncertainties of the BJH model calculations. The parent HZSM-5/γ-Al$_2$O$_3$ contained 0.12 cm^3/g micropores [28]. Although a slight narrowing of the micropore width was observed from the high-resolution Ar physisorption data (Figure S1a), the microporous volume remained similar after the addition of phosphorus and the steamed P/HZSM-5/γ-Al$_2$O$_3$, and HZSM-5/γ-Al$_2$O$_3$ had similar acidity (see Table 1 and Figure S2).

Table 1. Textural properties (determined by N$_2$ physisorption) and acidity of the different catalysts (steam-treated).

	P Content (wt%)	BET (m^2/g)	V_{meso} (cm^3/g)	V_{total} (cm^3/g)	Acidity (mmol NH$_3$/g)
HZSM-5/γ-Al$_2$O$_3$	-	376	0.32	0.45	0.39
P/HZSM-5/γ-Al$_2$O$_3$	0.41	381	0.28	0.41	0.40
γ-Al$_2$O$_3$	-	235	0.53	0.52	0.31

2.2. Product Yields

2.2.1. Light Gases

Figure 1 shows the gas yields for each vapor pulse at different constant catalyst temperatures using P/HZSM-5/γ-Al$_2$O$_3$ as a catalyst. Note that the yield of C$_1$-C$_3$ hydrocarbons has been multiplied by a factor of 10. At a higher constant catalyst temperature, an increase in the yields of all gas species was observed. However, the increase in CO$_2$ yield was less pronounced compared to CO. With an increased feeding of biomass, the yield of C$_2$-C$_3$ alkenes and C$_{4+}$ products (which include both saturated and unsaturated C$_4$ and C$_5$ hydrocarbons) continuously decreased, which is attributed to a decreased cracking activity of the catalyst and reduced activity of the hydrocarbon pool-type mechanistic cycle, producing not only monoaromatics, but also ethylene and propylene [50]. Propylene is a more valuable product compared to ethylene. The selectivity of propylene within the product group of C$_2$-C$_3$ alkenes increased from 54 mol% at 450 °C to 64 mol% at 500 °C. At temperatures of 550 and 600 °C, the propylene selectivity decreased to 48 and 43 mol%, respectively.
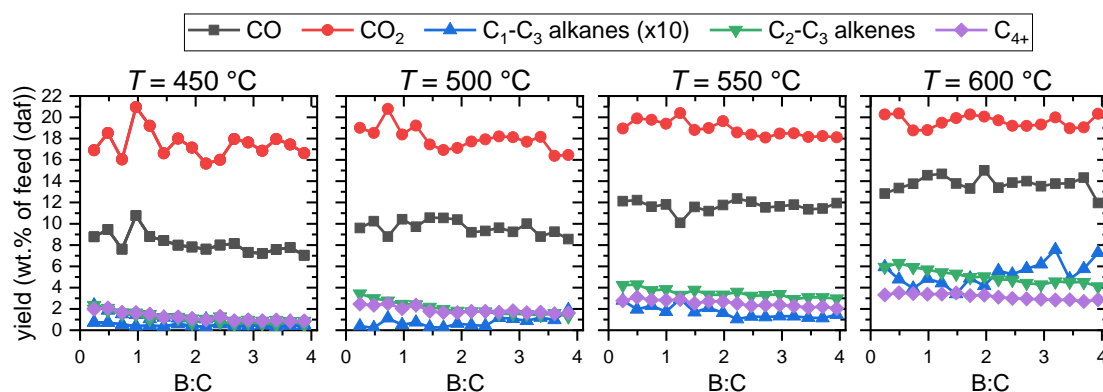
Figure 1. Change in momentary gas yields with increased biomass injection at constant temperatures (450, 500, 550, and 600 °C) of catalyst P/HZSM-5/γ-Al$_2$O$_3$. The yield of C$_1$-C$_3$ alkanes was multiplied by a factor of 10.

When the temperature was increased in between injections following the *T* profiles I and II (see Figure 2a,b, respectively), the CO$_2$ yields again remained fairly stable, whereas an increasing trend for the yield of the other light gases was observed. While the yield of alkenes increased more gradually with increasing temperature, the yield of C$_1$-C$_3$ alkanes increased, especially above ~540 °C, which is attributed to cracking reactions.
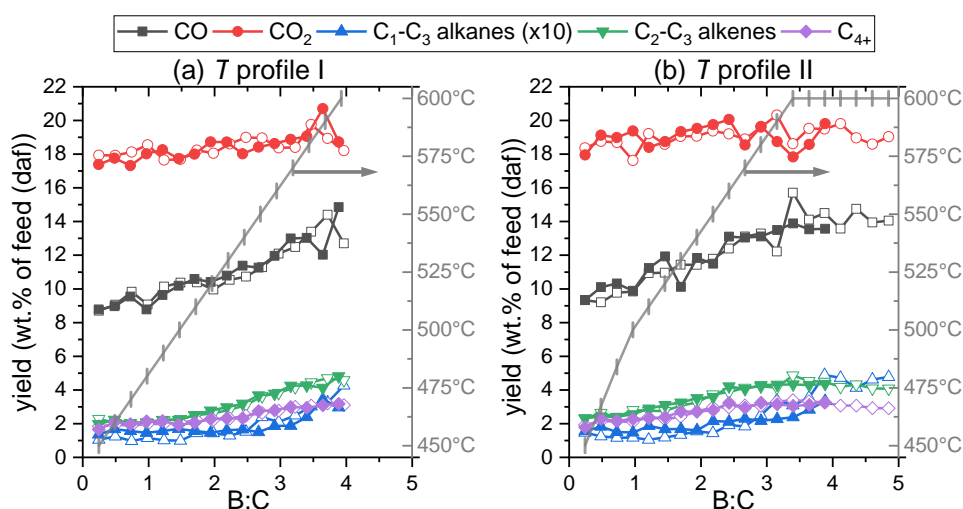

Figure 2. Change in momentary gas yields with increasing biomass injection when (**a**) increasing the catalyst temperature following temperature profile I, and (**b**) following temperature profile II. The yield of C$_1$-C$_3$ alkanes was multiplied by a factor of 10. Catalyst: P/HZSM-5/γ-Al$_2$O$_3$. Open symbols show results from replicate runs.

Similar trends in gas yields were observed using bare γ-Al$_2$O$_3$ as a catalyst (see Figure 3), however, with lower yields of hydrocarbons (in particular alkenes) compared to P/HZSM-5/γ-Al$_2$O$_3$. This is expected, since HZSM-5 is a known additive in FCC catalysts to increase propylene yields [51–53]. When following the *T* profile I during the catalytic upgrading, both CO and CO$_2$ yields continuously increased, while a more pronounced increase in the yield of light HC was observed at T > ~530 °C.
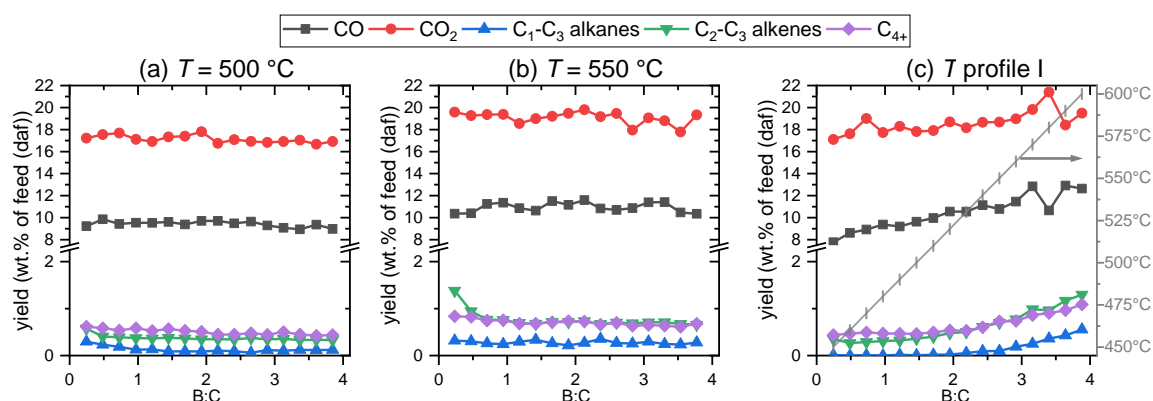
Figure 3. Change in momentary gas yields with increasing biomass injection for (**a**) a catalyst temperature of 500 °C, (**b**) a catalyst temperature of 550 °C, and (**c**) following temperature profile I. Catalyst: γ-Al_2O_3.

2.2.2. Vapors

Figure 4 provides an overview of the carbon yields of different vapor product groups (with respect to the fed carbon in biomass) at constant catalyst temperatures between 450 and 600 °C using P/HZSM-5/γ-Al_2O_3 as a catalyst. The carbon recovery of monoaromatics (MAR) rapidly declined at all temperatures, and most rapidly at 450 °C. With increasing catalyst temperatures, there was an increase in the initial yield of MAR, and a more pronounced yield of aliphatics (ALI), for which its yield of ~1 wt% C increased to ~4 wt% C. Towards higher temperatures, the breakthrough of many oxygenates, such as ketones (KET), furans (FUR), acids (AC), and methoxyphenols (MPH), was significantly delayed, as seen by lower slopes in the trajectories of the vapor yields, particularly below B:C ~2. The yield of phenolics (PH) reached a peak (shifted to higher B:C at higher catalyst T), after which its yield steadily declined, indicating the less effective removal of methoxy groups from lignin-derived methoxyphenols. In addition, phenolics may have been produced from the reaction of aromatic precursors from cellulose/hemicellulose-derived compounds with water and built up inside the catalyst pores as the catalyst aged [54]. The emergence of furans during HZSM-5 deactivation was also observed by others [55,56] and can be attributed to the incomplete deoxygenation and cracking of furfuryl alcohols (from cellulose and hemi-cellulose) and the decreased activity of Diels-Alder reactions between alkenes and biomass-derived furans [21].
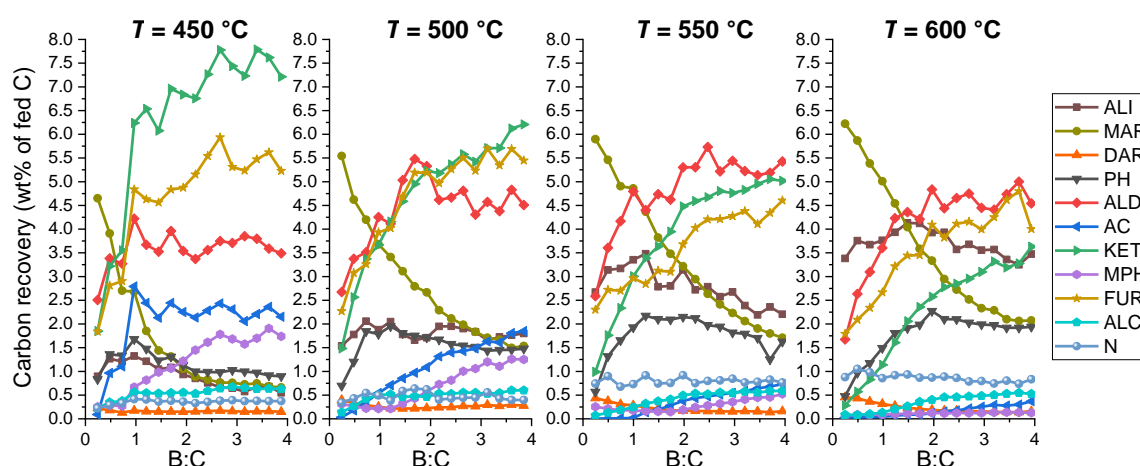

Figure 4. Carbon recovery of vapor products quantified by GC-FID when upgrading wheat straw pyrolysis vapors over P/HZSM-5/γ-Al_2O_3 at four different catalyst temperatures. The momentary yields per biomass injection are shown. Legend applies to all graphs.

Stanton et al. [56] recently investigated the role of biopolymers in the deactivation of HZSM-5 during the catalytic fast pyrolysis of cellulose, lignin, and pine using the same type of tandem μ-reactor as applied in the present study. While those researchers applied a similar flowrate of He carrier gas (54 mL/min) and biomass loading per injection (0.5 mg) compared to our work (60 mL/min He, 0.5 mg biomass (daf)), Stanton et al. [56] loaded a mass of catalyst five times higher (10 mg). In addition, in their work, a more acidic HZSM-5 with Si/Al = 15 was used without steam treatment prior to reaction with only 12% bentonite binder content, while in the present work, steam-treated ZSM-5 with Si/Al = 40 was used with 35% alumina binder. These deviations explain the higher conversion and complete deoxygenation observed by Stanton et al. at low B:C [56]; nevertheless, at B:C > 0.25, these researchers observed that the yield of oxygenates continuously increased at the expense of deoxygenated hydrocarbons. Due to the lower ratio of injected biomass per catalyst (g/g), 40 injections were needed in Stanton et al.'s work to reach B:C = 2. While the use of 2 mg of catalyst in the present work resulted in a lower conversion of oxygenates, the breakthrough of oxygenates and the decreasing yield of deoxygenated products was resolved well.

Figure 5 compares the carbon recovery of different product groups obtained in the present work when the temperature was increased in a constant manner (*T* profile I) or in an optimized manner (*T* profile II) using P/HZSM-5/γ-Al$_2$O$_3$ as a catalyst. With an increase in temperature following *T* profile I, the carbon recovery of MAR stabilized at B:C ~1.5, while the yield of ALI and PH continued to increase with increasing temperature. The yield of acids peaks at B:C ~1, while ketones increased up to B:C ~2 before the yield of both product groups decreased. This indicates that the applied temperature ramp more than compensates for the loss in activity for these species.
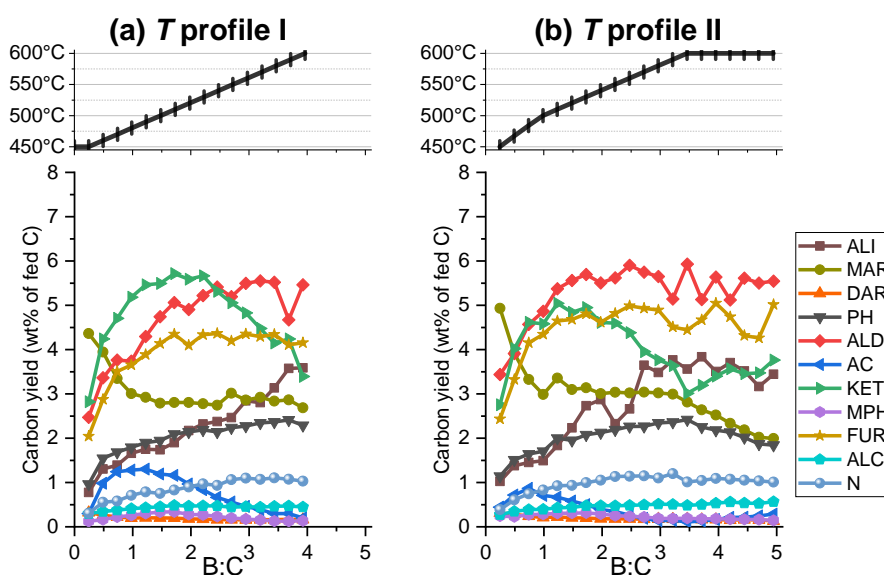

Figure 5. Carbon recovery of vapor products quantified by GC-FID when upgrading wheat straw pyrolysis vapors over P/HZSM-5/γ-Al$_2$O$_3$ following (**a**) a constant temperature increase of 10 °C per biomass injection and (**b**) an adapted temperature increase, as indicated above the graphs. The momentary carbon yields per biomass injection are shown. Legend applies to both graphs.

Following *T* profile II stabilized the yield of MAR at B:C ~1, however, at B:C > 3.25, the yield of MAR slowly decreased. Compared to results obtained with *T* profile I, the breakthrough of AC and KET could already be reversed at lower B:C ratios of 0.75 and 1.25, respectively. As a result, the carbon yield of acids was only 0.5 wt% at B:C ~4 for the optimized *T* profile II, while it was 0.9 wt% for *T* profile I.

Using γ-Al$_2$O$_3$ as a catalyst at 500 °C resulted in a rapid breakthrough of AC and MPH and a low yield of O-free hydrocarbons (Figure 6a). At 550 °C, in the initial upgrading phase, higher yields of

aliphatics and MAR were obtained, which rapidly declined until B:C ~1, followed by a slower rate of deactivation (Figure 6b). It is worth pointing out that, in contrast to the HZSM-5-containing catalyst, a higher selectivity of aliphatics compared to aromatics was obtained using γ-Al$_2$O$_3$. MPH conversion was considerably better at the elevated catalyst temperature, and also the breakthrough of AC was delayed (Figure 6b). Following *T* profile I reversed the breakthrough of AC, maintained a complete conversion of MPH up to B:C ~4, and produced slowly increasing yields of aromatics and aliphatics (see Figure 6c).
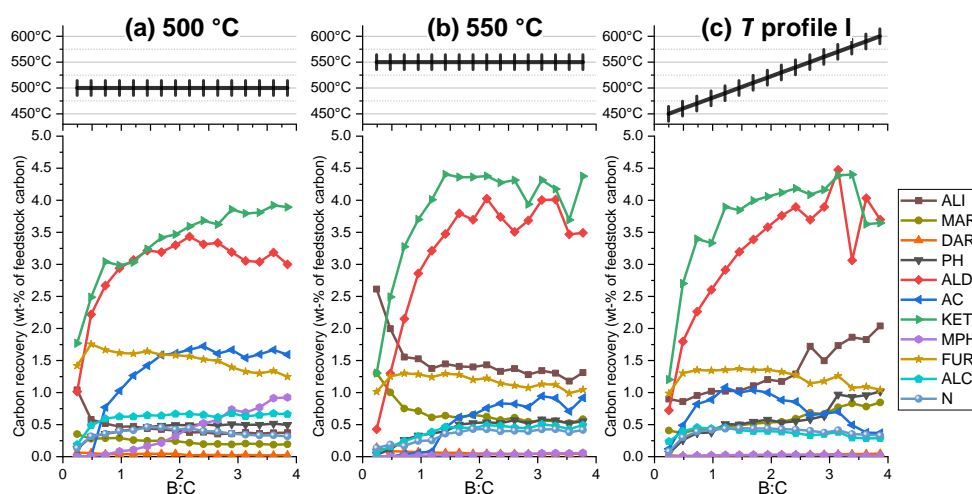

Figure 6. Carbon recovery of vapor products quantified by GC-FID when using γ-Al$_2$O$_3$ as a catalyst at temperatures of (**a**) 500 °C, (**b**) 550 °C, and (**c**) following *T*-profile I. The momentary carbon yields per biomass injection are shown. Legend applies to all graphs.

2.2.3. Coke

The coke combusted under an oxidizing atmosphere in the temperature range 350–650 °C, as shown by the differential thermogravimetric (DTG) curves in Figure 7. Coke on γ-Al$_2$O$_3$ combusted more readily (main weight loss around 475 °C), while the coke on P/HZSM-5/γ-Al$_2$O$_3$ that combusted at higher temperatures, is attributed to coke in the zeolite component [28,57].
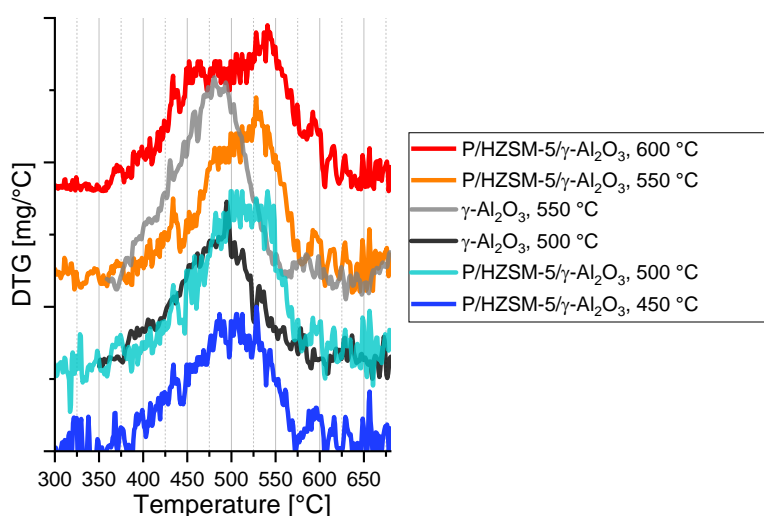

Figure 7. DTG curves from coke combustion after B:C ~4 using P/HZSM-5/γ-Al$_2$O$_3$ and γ-Al$_2$O$_3$. Curves obtained at different catalyst temperatures have been shifted vertically to facilitate comparison.

2.2.4. Cumulative Product Yields

Table 2 provides an overview of the carbon recovery of different product groups. Deoxygenated vapor products and alkenes are seen as desirable products, whereas CO, CO_2, light C_1-C_3 alkanes, and coke represent undesirable products.

Table 2. Cumulative carbon yield of products (wt% C of fed biomass carbon) for a final B:C ratio of ~4 (integration of 16 vapor pulses). The major product groups, i.e., gas, vapors, and coke are shown in bold. In addition, the detailed composition of the yield of aromatics is shown (from benzene to 3-ring aromatics).

Catalyst	SiC *	P/HZSM-5/γ-Al$_2$O$_3$						γ-Al$_2$O$_3$		
Temperature (°C)	500	450	500	550	600	profile (I)	profile (II)	500	550	profile (I)
Gas	**17.3**	**21.3**	**25.8**	**32.1**	**38.8**	**30.2**	**32.7**	**19.9**	**23.6**	**22.3**
CO	6.4	7.2	8.6	10.4	12.4	9.7	10.6	8.4	9.7	9.3
CO$_2$	9.7	9.9	10.2	10.7	10.9	10.4	10.8	9.7	10.8	10.5
C$_1$-C$_3$ alkanes	0.13	0.04	0.21	0.31	0.66	0.30	0.34	0.21	0.44	0.21
C$_2$-C$_3$ alkenes	0.5	1.9	3.6	6.2	9.3	5.5	6.2	0.7	1.4	1.1
C$_4$$^+$	0.6	2.2	3.4	4.5	5.6	4.3	4.8	0.9	1.2	1.1
Vapors	**16.3**	**21.5**	**22.7**	**23.7**	**21.6**	**21.1**	**23.4**	**11.6**	**12.1**	**12.1**
ALI	0.2	1.3	2.9	4.1	5.2	3.2	4.1	0.5	1.5	1.3
Aromatics	**0.1**	**1.6**	**3.3**	**3.9**	**4.3**	**3.3**	**3.6**	**0.3**	**0.7**	**0.6**
Benzene	0.0	0.1	0.3	0.4	0.5	0.3	0.4	0.1	0.1	0.1
Toluene	0.1	0.3	0.7	1.1	1.4	0.8	0.9	0.1	0.2	0.2
Xylenes	0.0	0.3	0.7	0.8	0.7	0.6	0.7	0.0	0.1	0.1
Alkyl-benzenes	0.1	0.3	0.6	0.4	0.3	0.4	0.5	0.0	0.1	0.1
Alkenyl-benzenes	0.0	0.2	0.3	0.3	0.4	0.3	0.3	0.0	0.0	0.1
Indanes	0.0	0.1	0.2	0.1	0.1	0.1	0.1	0.0	0.0	0.0
Indenes	0.0	0.2	0.3	0.4	0.4	0.3	0.3	0.0	0.2	0.1
2-ring aromatics	0.0	0.1	0.2	0.4	0.4	0.3	0.3	0.0	0.1	0.0
3-ring aromatics	0.0	0.0	0.0	0.1	0.1	0.1	0.0	0.0	0.0	0.0
PH	0.6	1.4	1.9	2.3	2.2	2.2	2.6	0.4	0.4	0.6
ALD	3.1	2.5	3.1	3.3	2.9	2.9	3.2	2.9	3.2	3.2
AC	2.2	2.8	1.5	0.4	0.1	0.9	0.5	1.3	0.5	0.7
KET	6.3	6.4	5.2	4.8	3.0	4.4	4.5	3.3	3.8	3.7
MPH	1.3	1.2	0.6	0.1	0.0	0.1	0.0	0.4	0.0	0.0
FUR	1.4	3.1	2.9	3.2	2.7	2.8	3.1	1.5	1.2	1.2
ALC	0.7	0.5	0.4	0.4	0.3	0.5	0.4	0.6	0.4	0.4
NIT	0.0	0.7	0.9	1.1	1.0	0.9	1.1	0.4	0.3	0.4
Coke	**0**	**5.9**	**6.9**	**6.6**	**8.2**	**7.7**	**6.9**	**5.7**	**7.2**	**8.6**
C-% closure †	65	80	87	94	100	90	93	68	74	74

* cumulative yields after four vapor pulses at B:C ~1; † The carbon recovery of char was ~31 wt% C for all tests.

Using P/HZSM-5/γ-Al$_2$O$_3$, the gas yields increased from 21.3 C% at 450 °C to 38.8 C% at 600 °C. Simultaneously, the yield of unreactive light C_1-C_3 alkanes increased from 0.04 to 0.66 C% and the

yield of valuable C_2-C_3 alkenes increased from 1.9 to 9.3 C%. Operating at higher catalyst temperatures increased the cumulative yield of MAR at B:C ~4 from 1.6 to 3.8 C%, and led to an increased yield of CO, polyaromatics, and coke (Table 2), in agreement with the literature [34]. At the higher temperatures, the extent of vapor deoxygenation increased and very low yields of AC and MPH resulted (Table 2). It is further worth noting that the carbon balance closure increased from 80% at 450 °C to 100% at 600 °C, which suggests that the missing carbon at low catalyst activity constitutes heavy matter, which did not reach the detectors and was deposited in the system [58,59]. With an increase in constant catalyst temperature from 450 to 550 °C, the carbon yield of GC-detectable vapors increased from 21.5 to 23.7%, before it decreased at higher temperatures of 600 °C (21.6%). The initial increase is attributed to the improved cracking and conversion of oligomeric primary vapors into volatile products, while the decrease at 600 °C likely resulted from the increased formation of light gases and coke, thereby reducing the yield of volatiles.

At constant catalyst temperatures of 500 and 550 °C, γ-Al_2O_3 produced considerably lower yields of alkenes and MAR (Table 2) compared to P/HZSM-5/γ-Al_2O_3. γ-Al_2O_3 was similarly effective in converting acids, and slightly more effective in converting MPH. Lower yields of FUR and KET resulted when using γ-Al_2O_3, and a generally lower carbon balance closure compared to the ZSM-5-containing catalyst resulted from significantly lower vapor yields (see Table 2) and suggests a low activity for converting heavy matter into GC-detectable vapors.

The cumulative yields obtained at B:C ~4 for P/HZSM-5/γ-Al_2O_3 when following temperature profile I were similar to the results obtained at constant catalyst temperatures of 500 and 550 °C (see Table 2). The accelerated increase in temperature in? the initial vapor processing stage of *T* profile II led to higher gas yields and increased vapor deoxygenation compared to results obtained with *T* profile I, with the results being similar to what was obtained at a constant catalyst temperature of 550 °C. Similarly, results obtained for γ-Al_2O_3 when following *T* profile I resembled the results obtained at a constant catalyst temperature of 550 °C, albeit at higher coke yields (8.6 vs. 7.2 C%). By increasing the catalyst activity with temperature, the obtained effect here, in a way, simulates an increased catalyst-to-biomass ratio, for which increased coke yields were reported [22].

From Table 2, it can be seen that the untreated vapors (SiC) already contained a high fraction of ketones, and the treated vapors still contained a high contribution of ketones. This, however, does not distinguish between ketones with multiple/mixed oxygen functionalities and simple ketones with a single ketone group. The vapor product groups were therefore further combined into three groups according to their number of oxygen atoms; that is, into hydrocarbons with zero oxygen atoms, one oxygen atom, and two or more oxygen atoms. Figures 8–10 show the momentary yields per biomass injection of these three major vapor product groups and Figure 11 provides an overview of the cumulative product yields at the final B:C ratio. Comparing the trajectories of the grouped product yields at different constant catalyst temperatures using P/HZSM-5/γ-Al_2O_3 (Figure 8) shows that the initial yield of oxygen-free hydrocarbons could be doubled (from ~3 to 6 wt%) when increasing the catalyst temperature from 450 °C to 600 °C. At 450 °C, highly oxygenated compounds with two or more oxygen atoms rapidly broke through towards higher B:C ratios, whereas they were much better converted at higher temperatures, which can be attributed to an increased catalyst activity. Additionally, for simple oxygenates, a more gradual breakthrough occurred at higher catalyst temperatures up to B:C ~2 before reaching a plateau, while at 450 °C, the plateau was already reached at B:C ~1. From this, it is clear that a higher catalyst temperature provided a lower proportion of oxygenates, which decreased the oxygen content of the accumulated vapors at B:C ~4 from 29.6 (at 450 °C) to 15.6 wt% (at 600 °C) (Table 3, Figure 11). While the vapors treated with inactive SiC hardly contained oxygen-free hydrocarbons, their cumulative yield at B:C ~4 increased from 2.0 (450 °C) to 5.9 wt% (600 °C) when using a P-modified HZSM-5/Al_2O_3 catalyst (Figure 11). The catalytic vapor treatment increased the yield of simpler one-oxygen products, such as phenols, alcohols, and furans, compared to the non-catalytic reference (3.7 wt%), which is attributed to the partial deoxygenation of highly oxygenated groups. With increases in temperature from 450 °C to 500 °C and 550 °C, the yield of

simpler one-oxygen products increased from 7.9 to 9.1 and 9.5 wt%, and decreased to 7.7 wt% upon a further temperature increase to 600 °C (Figure 11). This indicates that one-oxygen groups are more difficult to deoxygenate and require a higher catalyst activity to remove oxygen (e.g., a high dissociation energy of 468 kJ/mol for the breakage of the C-O bond in phenol [60]).
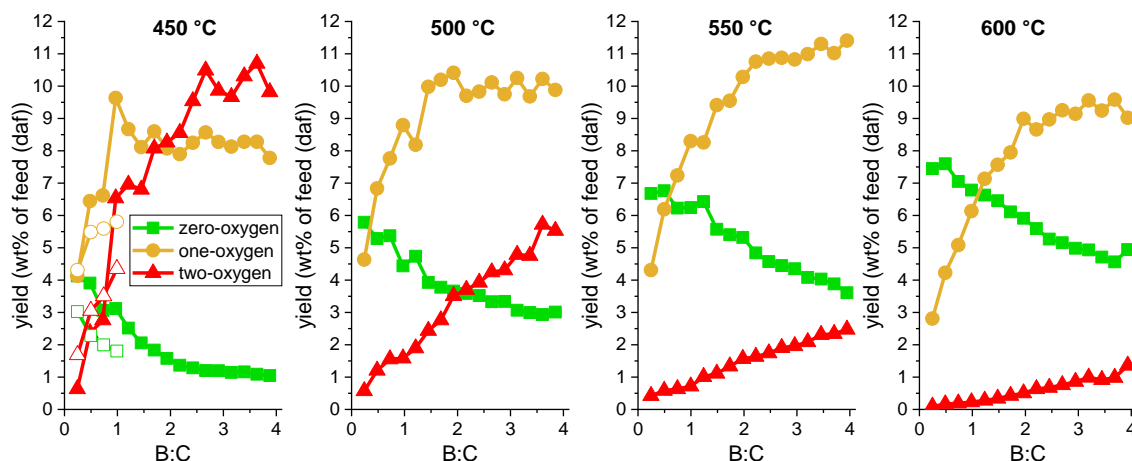

Figure 8. Yields (wt% of fed biomass (daf)) of hydrocarbons containing zero, one, and two or more oxygen atoms for upgrading over P/HZSM-5/γ-Al$_2$O$_3$ at different constant catalyst temperatures. The momentary yields obtained at each biomass injection as a function of increasing cumulative B:C ratio are shown. Open symbols in the left graph were obtained for repeated runs with a new catalyst to B:C ~1. Legend applies to all graphs.
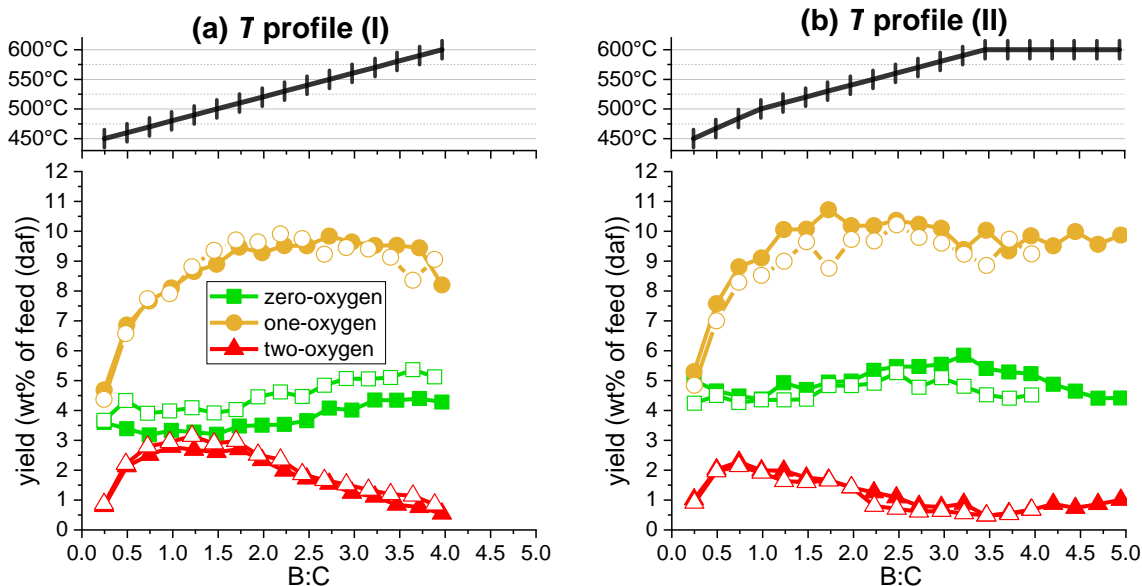

Figure 9. Yields (wt% of fed biomass (daf)) of hydrocarbons containing zero, one, and two or more oxygen atoms for upgrading over P/HZSM-5/γ-Al$_2$O$_3$ at (**a**) temperature profile I and (**b**) at temperature profile II. The momentary yields obtained at each biomass injection as a function of increasing cumulative B:C ratio are shown. Open symbols show yields obtained from replicate runs with a new catalyst.
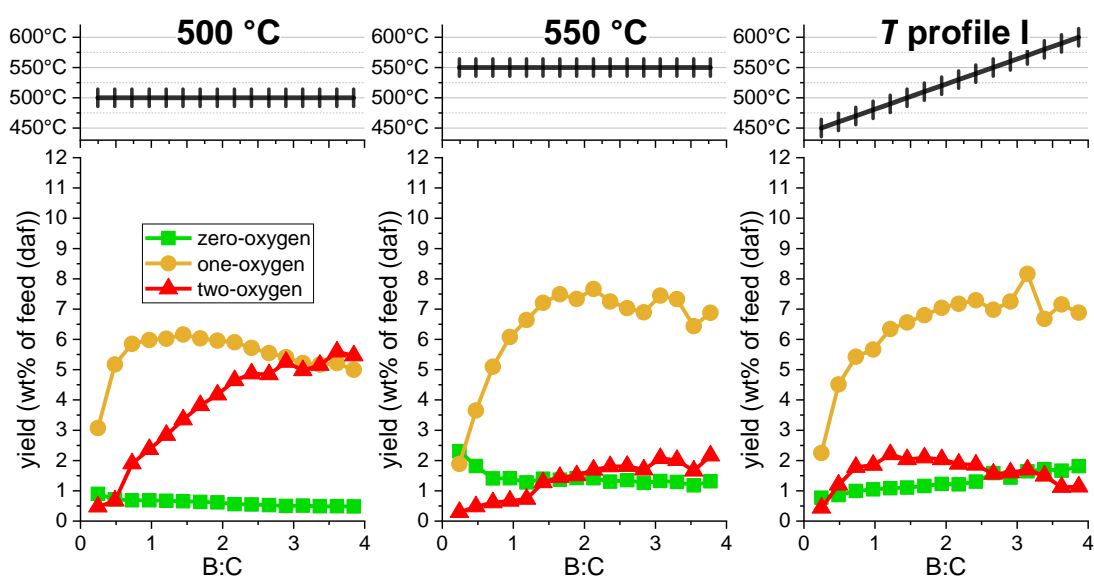
Figure 10. Yields (wt% of fed biomass (daf)) of hydrocarbons containing zero, one, and two or more oxygen atoms for upgrading over γ-Al$_2$O$_3$ at constant temperatures of 500 and 550 °C or following temperature profile I. The momentary yields obtained at each biomass injection as a function of increasing cumulative B:C ratio are shown.
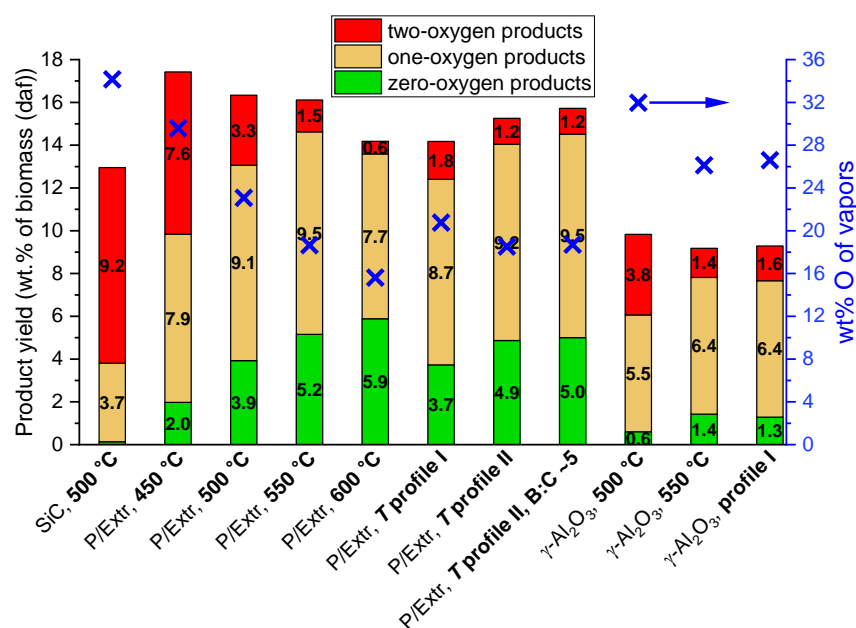

Figure 11. Product yield of vapor compounds grouped as containing zero oxygen atoms, one oxygen atom, or two oxygen atoms. The cumulative yields at B:C ~4, unless indicated otherwise (B:C ~5 for one test), are shown. P/Extr refers to P/HZSM-5/γ-Al$_2$O$_3$.

Table 3. Properties of the accumulated non-condensed vapors at the indicated B:C ratios that are important for fuel applications. In addition, the atomic CO/CO_2 ratio in the gas is shown.

Catalyst	T (°C)	B:C	EHI	H/C	O/C	HHV (MJ/kg)	wt% O	Gas Atom. CO/CO_2 Ratio
SiC	500	1	0.65	1.71	0.53	24.1	34.2	0.66
HZSM-5/γ-Al$_2$O$_3$	500	4	0.97	1.46	0.24	31.7	22.2	1.22
P/HZSM-5/γ-Al$_2$O$_3$	450	4	0.82	1.54	0.36	28.0	29.6	0.73
	500	4	0.98	1.50	0.26	31.4	23.1	0.84
	550	4	1.07	1.47	0.20	33.7	18.7	0.97
	600	4	1.15	1.47	0.16	35.4	15.6	1.15
	profile I *	4	1.02	1.47	0.23	32.6	20.8	0.94
	profile II *	4	1.10	1.47	0.20	33.8	18.5	0.97
	profile II *	5	1.09	1.47	0.20	33.70	18.7	0.98
γ-Al$_2$O$_3$	500	4	0.89	1.71	0.41	27.3	32.0	0.86
	550	4	1.08	1.69	0.31	30.6	26.1	0.90
	profile I *	4	1.05	1.68	0.32	30.2	26.6	0.88

* see Section 4.5 for a detailed explanation of the applied temperature profiles.

A quite different trajectory of product yields resulted when gradually increasing the catalyst temperature for each injection (*T* profile I), as shown in Figure 9a. A more stable yield of oxygen-free hydrocarbons was obtained, which even slightly increased towards higher temperatures (B:C ~3–4). The yields of compounds with two or more oxygen atoms reached a plateau at B:C ~1.5 (*T* = 500 °C) before continuously decreasing with further increases in temperature. This demonstrates that the breakthrough of highly oxygenated products can be successfully prevented by compensating the loss in activity due to coking by the temperature-facilitated increase in activity.

By increasing the temperature at a higher rate between 450 and 500 °C following temperature profile II (Figure 9b), the breakthrough of highly oxygenated compounds could be reversed earlier, at B:C ~0.75, and continue to decrease when increasing the temperature to 600 °C. When maintaining the catalyst temperature at 600 °C during the last seven injections (B:C = 3.5–5.0), the yield of oxygen-free hydrocarbons slightly decreased and the yield of compounds with two oxygen atoms slightly increased (Figure 9b). The initially accelerated temperature increase in profile II aimed to mirror the rapid decrease in catalyst acidity due to coking [30,34], and resulted in a decrease in the oxygen content of the accumulated vapors from 20.8 to 18.5% due to a slightly increased yield of oxygen-free HC and a decreased yield of two-oxygen-containing products (Figure 11). An important benefit of the presented strategy is that it allows operation at higher B:C ratios without leading to a pronounced increase in oxygen content (Figure 11). At the elevated catalyst temperature of 600 °C, the most reactive oxygenates were converted even at B:C > 4, and there was virtually no change in the oxygen content of the cumulative vapors at B:C ~4 (18.5 wt%) and B:C ~5 (18.7 wt%). The presented approach would thereby reduce the regeneration frequency in a process concept with parallel fixed beds and therefore the number of required fixed bed reactors, with associated benefits, such as reduced process complexity and investment costs (both equipment and catalyst inventory) [26,61].

Figure 10 shows the momentary yields of hydrocarbons containing zero, one, and two or more oxygen atoms for upgrading over γ-Al$_2$O$_3$ at constant catalyst temperatures of 500 and 550 °C, and when following *T* profile I. Lower yields of oxygen-free hydrocarbons obtained with γ-Al$_2$O$_3$ compared to P/HZSM-5/γ-Al$_2$O$_3$ are predominantly due to lower yields of monoaromatics (see Table 2).

Similar to the observations made at constant temperatures using P/HZSM-5/γ-Al$_2$O$_3$ as a catalyst, an increased catalyst temperature of 550 °C slowed down the breakthrough of highly oxygenated compounds compared to a constant catalyst temperature of 500 °C. By following a constant increase in temperature (profile I) during the vapor upgrading, the yield of highly oxygenated compounds (especially acids) reached a plateau at B:C ~1.5 before decreasing towards a higher temperature—similar to the observations made for P/HZSM-5/γ-Al$_2$O$_3$ (Figure 9a). Based on this, it appears highly likely that following a temperature profile with an initially accelerated increase, similar to profile II, will allow operation at higher B:C ratios and maintain lower concentrations of AC and MPH compared to operating at a constant catalyst temperature.

This illustrates that the concept of counteracting the loss in activity by increasing the temperature can also be applied to low-cost catalysts such as γ-Al$_2$O$_3$. However, the rate of the required temperature increase will need to be optimized depending on the catalyst and process conditions, and in particular, it will depend on the rate of catalyst deactivation, the ratio of catalyst loading to biomass feeding rate (W/F), and the catalyst contact time.

It is worth mentioning that, compared to HZSM-5, which is prone to thermal degradation at temperatures higher than 600 °C [62] and dealumination in severe hydrothermal conditions, a high stability up to ~750 °C is expected for γ-Al$_2$O$_3$ [63]. This may allow the extension of the vapor upgrading with hydrothermally stable metal oxides to a higher B:C by slowly increasing the temperature even beyond 600 °C, as long as gas formation does not become excessive.

2.3. Product Quality

With increasing catalyst temperatures, the molar CO/CO$_2$ ratio increased when using P/HZSM-5/γ-Al$_2$O$_3$ (Table 3). In addition, the carbon recovery of monoaromatics, coke, and C$_{2/3}$ alkenes increased (Table 2). Since decarbonylation reduces the carbon efficiency (loss of one carbon atom per removed oxygen atom) and little increase in monoaromatic yield is observed when increasing the catalyst temperature > 550 °C, the range of optimal (constant) catalyst operation appears to be 500–550 °C.

To investigate if the approach of ramping the reaction temperature limited the carbon losses to C$_1$-C$_3$ alkanes, their yields were plotted against the extent of achieved vapor deoxygenation (Figure S3). Using P/HZSM-5/γ-Al$_2$O$_3$ as a catalyst, similar losses to C$_1$-C$_3$ alkanes resulted compared to maintaining a constant catalyst temperature (Figure S3). For γ-Al$_2$O$_3$, on the other hand, at a similar level of deoxygenation, the yield of C$_1$-C$_3$ alkanes was less than half when following *T* profile I compared to operating at 550 °C (see Table 2 and Figure S3).

3. Discussion

The approach of incomplete catalyst regeneration suggested by others [32], in order to decrease high carbon losses to coke in the initial upgrading period, suits configurations of short catalyst contact time, e.g., a riser reactor for cracking the oxygenates coupled to a fluidized bed oxidative regenerator. When upgrading the vapors over a fixed bed, however, it is unlikely to obtain a homogenous level of incomplete regeneration along the bed due to difficult-to-control variations in oxygen concentration and bed temperature along the bed. Fixed bed reactors are commonly operated using an excess of catalyst. While this ensures high conversion, higher catalyst loadings also lead to higher coke yields [27], which might be attributed to an "over-cracking" and the further reaction of the deoxygenated vapors. As an example, fully deoxygenated products, such as toluene, might encounter other strong acid sites further down the catalytic bed, leading to coke formation. With the demonstrated strategy, the catalyst activity and conversion of the pyrolysis vapors is controlled by the adjustment of the reactor temperature, which avoids the need for excessive catalyst loadings. Furthermore, starting the vapor upgrading over a catalyst with moderate activity (at a lower catalyst temperature) likely attenuates the extent of the trapping of already deoxygenated products, such as coke, but further research is needed to investigate this aspect.

To adjust the catalyst bed temperature of a continuous process, on-line measurements of one or several markers should preferably be carried out and applied in a control procedure to keep these at a specified low concentration in the product. It could, for example, be to ensure that there are no two-oxygen products, and/or no acids, etc.

4. Materials and Methods

4.1. Biomass

Wheat straw with a particle size of 0.1–0.25 mm was used as feedstock. Its properties were reported in more detail in earlier work [58]. The moisture content (as received) was 7.1 wt%, and the volatiles, fixed carbon, and ash on a dry basis (d.b.) amounted to 74.4 wt%, 15.8 wt%, and 9.8 wt%, respectively. Compositional ash analysis obtained from the same feedstock (particle range 0–1.4 mm) has been reported earlier [27]. The content of N, C, H, S, and O (by difference) of the biomass feedstock on a dry and ash-free basis (daf) was 1.3, 48.2, 5.0, 0.1, and 45.4, respectively.

4.2. Catalyst Preparation

Extrudates of HZSM-5/γ-Al$_2$O$_3$ and γ-Al$_2$O$_3$ were provided by Haldor Topsoe A/S. For impregnation with phosphorus, the extrudates were crushed and mixed in a 1:10 weight ratio with Milli-Q water containing the required amount of phosphorus, which was added in the form of H$_3$PO$_4$ (85 wt%, Honeywell Fluka). The slurry was heated in a rotary evaporator at 80 °C and 180 rpm and the water was slowly removed by decreasing the pressure. After drying overnight at 105 °C, the P-modified HZSM-5/γ-Al$_2$O$_3$ extrudate (P/Extr) was heated to 500 °C at 2.6 K/min and conditioned for 3 h in a flow of synthetic air in a calcination oven. After calcination, the catalyst was steam treated at atmospheric pressure (0.3 bar H$_2$O) for 5 h at 500 °C in order to accelerate the initial loss in acidity by dealumination [64]. This allowed the deactivation during the reaction tests to be unambiguously attributed to coking. For consistency, the same conditions for steaming were applied to the bare γ-Al$_2$O$_3$, even though the steam treatment did not markedly affect its acidity [28].

4.3. Catalyst Characterization

The textural properties of the catalysts after degassing at 350 °C in vacuum were determined by applying N$_2$ physisorption and Ar physisorption in a Novatouch and AsiQ apparatus (3P instruments), respectively, as further described in earlier work [64]. Temperature programmed desorption (TPD) of NH$_3$ was performed using a Micromeritics Autochem II 2920 instrument, following the procedure described in [65]. The phosphorus content of P/HZSM-5/γ-Al$_2$O$_3$ was determined by X-ray fluorescence (XRF) [35].

4.4. Micro-Pyrolyzer

A tandem micro-pyrolysis system (Rx-3050tr, Frontier Labs, Japan), equipped with an auto-shot sampler (AS-1020E), was used in this work and the formed vapors were analyzed by gas chromatography (GC) coupled to mass chromatography (MS), flame ionization detector (FID), and thermal conductivity detector (TCD) (see Figure S4). The helium flowrate was 60 mL/min and the split ratio at the GC injection port was 56:1. The micro-pyrolyzer and the gas chromatographic conditions were described in more detail in earlier work [58]. The pyrolysis reactor temperature was controlled to 530 °C, and 0.59 ± 0.01 mg biomass was placed into stainless steel sample cups, secured with quartz wool, and subsequently dropped into the pyrolysis zone by the autosampler. The carrier gas swept the evolved pyrolysis vapors from the pyrolysis reactor to the catalytic reactor, which contained a quartz tube loaded with a mixture of 60 mg acid-washed and calcined quartz beads (150–215 μm) and 2 mg catalyst (36–125 μm). The catalyst bed was secured in between two quartz wool plugs and placed within the temperature-controlled isothermal zone of the catalytic reactor. Different temperatures of the catalytic reactor between 450 and 600 °C were investigated, as detailed in Section 4.5.

The light gases were quantified by TCD and grouped into CO, CO_2, C_1-C_3 alkanes, C_2-C_3 alkenes, and C_4-C_5 alkanes/alkenes. The vapor products were identified by MS and quantified by FID following the method explained in [27], which used external standards to obtain a linear correlation between the FID response factor and the chemical composition of a compound [66]. This in turn allowed the estimation of the FID response for compounds that were not directly calibrated for based on their chemical composition. The vapor products identified by FID were grouped into aliphatics (ALI), monoaromatics (MAR), 2–4 ring aromatics (DAR+), phenols (PH), aldehydes (ALD), acids (AC), ketones (KET), methoxyphenols (MPH), furans (FUR), alcohols (ALC), and nitrogen-containing compounds (NIT). The average content (wt%) of X = H, O, N, and C of the GC-identified vapors was calculated as wt% $X = \frac{\text{mass of X in vapors}}{\text{mass of vapors}}$, and the effective hydrogen index (EHI) of the vapors was calculated according to $EHI = \frac{H-2O-3N}{C}$ [67] with H, O, N, and C corresponding to the mole of each element in the sum of the identified vapor compounds. No sulfur compounds were detected. Based on the elemental composition of the vapors, their higher heating value was calculated [68].

Once catalyst testing was completed, the reactor was allowed to cool before removing the catalyst. The spent catalyst was emptied into alumina crucibles and the coke was combusted in a thermogravimetric analyzer (Netzsch STA449 F1 coupled with QMS 403 D Aëolos®), according to conditions described previously [58].

4.5. Test Conditions

Initial tests were performed with SiC as a highly inert solid at 500 °C and steamed HZSM-5/γ-Al_2O_3 extrudate at 500 °C for reference to investigate the effect of phosphorus impregnation. The steamed P-modified HZSM-5/γ-Al_2O_3 extrudate was tested at four different constant catalyst temperatures of 450, 500, 550, and 600 °C, and two different temperature ramps, which will be referred to as *T* profile I and *T* profile II, respectively:

- *T* profile I: Starting from a temperature of 450 °C, the catalyst temperature was increased by 10 °C in between each injection (corresponding to delta B:C ~0.25) until reaching 600 °C at the 16th injection (at B:C ~4).
- *T* profile II: Starting from a temperature of 450 °C, the catalyst temperature was increased by 16.7 °C per injection for the first three injections (until reaching 500 °C), followed by a 10 °C increase per injection for the next ten injections and holding the temperature at 600 °C for the remaining injections. An additional test was completed with continued biomass feeding until reaching B:C ~5 while holding the temperature at 600 °C.

The repeated injection over an empty catalyst reactor or SiC indicated a high reproducibility of the results [58]. While the reported results at constant catalyst temperatures were obtained from single test runs (16 injections), the tests with variable catalyst temperatures were performed in duplicate and the presented results constitute the averaged values. For the bare γ-Al_2O_3, a constant catalyst temperature of 500 and 550 °C was compared to results obtained following *T* profile I. Bench-scale investigations [27] showed that carbon losses to coke and gas severely diminished the recovery of upgraded bio-oil at low B:C, which is why B:C ~4 (reached after 16 injections) was chosen as a base case for the present work using the micro-pyrolyzer.

5. Conclusions

Phosphorus-modified HZSM-5/γ-Al_2O_3 extrudates and γ-Al_2O_3 were used as catalysts for the ex situ deoxygenation of wheat straw pyrolysis vapors. At different (constant) catalyst temperatures, the trajectories of the vapor and gas product yields were compared during catalyst deactivation up to B:C ~4, i.e., during 16 consecutive pyrolysis vapor pulses. At a lower catalyst temperature (450 °C), a rapid breakthrough of oxygenates with two or more oxygen atoms was observed, while this breakthrough was significantly delayed and/or occurred at a lower rate when vapor deoxygenation was performed at higher (constant) catalyst temperatures. The oxygen content of the cumulative

vapors decreased from 30.4 wt% to 17.5 wt%, and the yield of oxygen-free hydrocarbons (not including light gases) increased from 1.6 wt% to 4.6 wt% of fed biomass for vapor upgrading at 600 °C compared to 450 °C. In addition, the yield of light gases (especially CO and alkenes) and coke increased.

The loss in activity and the associated breakthrough of oxygenates could be successfully counteracted by raising the reaction temperature during the biomass feeding. This reversed the breakthrough of oxygenates and led to a more stable production of oxygen-free hydrocarbons. Furthermore, this approach allowed operation at higher B:C ratios while maintaining a good deoxygenation performance, which would in turn reduce the frequency of regeneration. The presented approach appears particularly interesting for catalysts that are robust under hydrothermal conditions. Additionally, for bare γ-Al_2O_3 as a hydrothermally stable low-cost alternative, catalytic deoxygenation activity could be maintained/improved by continuously increasing the catalyst temperature during the vapor treatment.

The results of this microscale study indicate that, by matching the loss in catalyst activity due to coking with an increased activity by increasing the catalyst temperature, the catalytic fast pyrolysis process can be optimized towards a more stable production of oxygen-free hydrocarbons. Since the GC-quantified yield of volatiles in the present work might not necessarily correlate with the yield in whole bio-oil, further investigations at larger scales are needed in order to compare the bio-oil yield and quality obtained at different constant catalyst temperatures to the results obtained at a carefully tuned increasing temperature depending on the rate of catalyst deactivation.

Author Contributions: Conceptualization, A.D.J. and A.E.; Funding acquisition, J.A.; Investigation, A.E.; Resources, B.H.S.; Visualization, A.E.; Writing—original draft, A.E.; Writing—review and editing, A.S., B.H.S., J.A., U.B.H., U.V.M., and A.D.J. All authors have read and agreed to the published version of the manuscript.

References

1. Bridgwater, A.V. Review of fast pyrolysis of biomass and product upgrading. *Biomass and Bioenergy* **2011**, *38*, 68–94. [CrossRef]

2. Sharifzadeh, M.; Sadeqzadeh, M.; Guo, M.; Borhani, T.N.; Konda, N.V.S.N.M.; Garcia, M.C.; Wang, L.; Hallett, J.; Shah, N. The multi-scale challenges of biomass fast pyrolysis and bio-oil upgrading: Review of the state of art and future research directions. *Prog. Energy Combust. Sci.* **2019**, *71*, 1–80. [CrossRef]

3. Krutof, A.; Hawboldt, K.A. Upgrading of biomass sourced pyrolysis oil review: Focus on co-pyrolysis and vapour upgrading during pyrolysis. *Biomass Convers. Biorefin.* **2018**, *8*, 775–787. [CrossRef]

4. Ruddy, D.A.; Schaidle, J.A.; Ferrell, J.R., III; Wang, J.; Moens, L.; Hensley, J.E. Recent advances in heterogeneous catalysts for bio-oil upgrading via "ex situ catalytic fast pyrolysis": Catalyst development through the study of model compounds. *Green Chem.* **2014**, *16*, 454–490. [CrossRef]

5. Stefanidis, S.D.; Kalogiannis, K.G.; Iliopoulou, E.F.; Lappas, A.A.; Pilavachi, P.A. In-situ upgrading of biomass pyrolysis vapors: Catalyst screening on a fixed bed reactor. *Bioresour. Technol.* **2011**, *102*, 8261–8267. [CrossRef] [PubMed]

6. Iliopoulou, E.F.; Stefanidis, S.D.; Kalogiannis, K.; Psarras, A.C.; Delimitis, A.; Triantafyllidis, K.S.; Lappas, A.A. Pilot-scale validation of Co-ZSM-5 catalyst performance in the catalytic upgrading of biomass pyrolysis vapours. *Green Chem.* **2014**, *16*, 662–674. [CrossRef]

7.   Williams, P.T.; Horne, P.A. The influence of catalyst regeneration on the composition of zeolite-upgraded biomass pyrolysis oils. *Fuel* **1995**, *74*, 1839–1851. [CrossRef]

8.   Iisa, K.; French, R.J.; Orton, K.A.; Dutta, A.; Schaidle, J.A. Production of low-oxygen bio-oil via ex situ catalytic fast pyrolysis and hydrotreating. *Fuel* **2017**, *207*, 413–422. [CrossRef]

9.   Williams, P.T.; Nugranad, N. Comparison of products from the pyrolysis and catalytic pyrolysis of rice husks. *Energy* **2000**, *25*, 493–513. [CrossRef]

10. Hernando, H.; Fermoso, J.; Ochoa-Hernández, C.; Opanasenko, M.; Pizarro, P.; Coronado, J.M.; Čejka, J.; Serrano, D.P. Performance of MCM-22 zeolite for the catalytic fast-pyrolysis of acid-washed wheat straw. *Catal. Today* **2018**, *304*, 30–38. [CrossRef]

11. Hernando, H.; Hernández-Giménez, A.M.; Gutiérrez-Rubio, S.; Fakin, T.; Horvat, A.; Danisi, R.M.; Pizarro, P.; Fermoso, J.; Heracleous, E.; Bruijnincx, P.C.A.; et al. Scaling-Up of Bio-Oil Upgrading during Biomass Pyrolysis over ZrO$_2$/ZSM-5-Attapulgite. *ChemSusChem* **2019**, *12*, 2428–2438. [CrossRef]

12. Mohammed, I.Y.; Kazi, F.K.; Yusup, S.; Alaba, P.A.; Sani, Y.M.; Abakr, Y.A. Catalytic intermediate pyrolysis of Napier grass in a fixed bed reactor with ZSM-5, HZSM-5 and zinc-exchanged zeolite-a as the catalyst. *Energies* **2016**, *9*, 246. [CrossRef]

13. Sun, L.; Zhang, X.; Chen, L.; Zhao, B.; Yang, S.; Xie, X. Comparision of catalytic fast pyrolysis of biomass to aromatic hydrocarbons over ZSM-5 and Fe/ZSM-5 catalysts. *J. Anal. Appl. Pyrolysis* **2016**, *121*, 342–346. [CrossRef]

14. Du, S.; Sun, Y.; Gamliel, D.P.; Valla, J.A.; Bollas, G.M. Catalytic pyrolysis of miscanthus×giganteus in a spouted bed reactor. *Bioresour. Technol.* **2014**, *169*, 188–197. [CrossRef]

15. Jae, J.; Tompsett, G.A.; Foster, A.J.; Hammond, K.D.; Auerbach, S.M.; Lobo, R.F.; Huber, G.W. Investigation into the shape selectivity of zeolite catalysts for biomass conversion. *J. Catal.* **2011**, *279*, 257–268. [CrossRef]

16. Carlson, T.R.; Tompsett, G.A.; Conner, W.C.; Huber, G.W. Aromatic production from catalytic fast pyrolysis of biomass-derived feedstocks. *Top. Catal.* **2009**, *52*, 241–252. [CrossRef]

17. Saraeian, A.; Nolte, M.W.; Shanks, B.H. Deoxygenation of biomass pyrolysis vapors: Improving clarity on the fate of carbon. *Renew. Sustain. Energy Rev.* **2019**, *104*, 262–280. [CrossRef]

18. Stöcker, M. Biofuels and biomass-to-liquid fuels in the biorefinery: Catalytic conversion of lignocellulosic biomass using porous materials. *Angew. Chemie Int. Ed.* **2008**, *47*, 9200–9211. [CrossRef]

19. Charoenwiangnuea, P.; Maihom, T.; Kongpracha, P.; Sirijaraensre, J.; Limtrakul, J. Adsorption and decarbonylation of furfural over H-ZSM-5 zeolite: A DFT study. *RSC Adv.* **2016**, *6*, 105888–105894. [CrossRef]

20. Foster, A.J.; Jae, J.; Cheng, Y.; Huber, G.W.; Lobo, R.F. Optimizing the aromatic yield and distribution from catalytic fast pyrolysis of biomass over ZSM-5. *Appl. Catal. A Gen.* **2012**, *423–424*, 154–161. [CrossRef]

21. Cheng, Y.T.; Huber, G.W. Production of targeted aromatics by using Diels-Alder classes of reactions with furans and olefins over ZSM-5. *Green Chem.* **2012**, *14*, 3114–3125. [CrossRef]

22. Patel, H.; Hao, N.; Iisa, K.; French, R.J.; Orton, K.A.; Mukarakate, C.; Ragauskas, A.J.; Nimlos, M.R. Detailed Oil Compositional Analysis Enables Evaluation of Impact of Temperature and Biomass-to-Catalyst Ratio on ex Situ Catalytic Fast Pyrolysis of Pine Vapors over ZSM-5. *ACS Sustain. Chem. Eng.* **2020**, *8*, 1762–1773. [CrossRef]

23. Carlson, T.R.; Jae, J.; Lin, Y.C.; Tompsett, G.A.; Huber, G.W. Catalytic fast pyrolysis of glucose with HZSM-5: The combined homogeneous and heterogeneous reactions. *J. Catal.* **2010**, *270*, 110–124. [CrossRef]

24. Carlson, T.R.; Cheng, Y.; Jae, J.; Huber, G.W. Production of green aromatics and olefins by catalytic fast pyrolysis of wood sawdust. *Energy Environ. Sci.* **2011**, *4*, 145–161. [CrossRef]

25. Lazaridis, P.A.; Fotopoulos, A.P.; Karakoulia, S.A. Catalytic Fast Pyrolysis of Kraft Lignin With Conventional, Mesoporous and Nanosized ZSM-5 Zeolite for the Production of Alkyl-Phenols and Aromatics. *Front. Chem.* **2018**, *6*, 295. [CrossRef]

26. Dutta, A.; Schaidle, J.A.; Humbird, D.; Baddour, F.G.; Sahir, A. Conceptual Process Design and Techno-Economic Assessment of Ex Situ Catalytic Fast Pyrolysis of Biomass: A Fixed Bed Reactor Implementation Scenario for Future Feasibility. *Top. Catal.* **2016**, *59*, 2–18. [CrossRef]

27. Eschenbacher, A.; Jensen, P.A.; Henriksen, U.B.; Ahrenfeldt, J.; Li, C.; Duus, J.Ø.; Mentzel, U.V.; Jensen, A.D. Impact of ZSM-5 deactivation on bio-oil quality during upgrading of straw derived pyrolysis vapors. *Energy Fuels* **2019**, *33*, 397–412. [CrossRef]

28. Eschenbacher, A.; Jensen, P.A.; Henriksen, U.B.; Ahrenfeldt, J.; Li, C.; Duus, J.Ø.; Mentzel, U.V.; Jensen, A.D. Deoxygenation of wheat straw fast pyrolysis vapors using HZSM-5, Al$_2$O$_3$, HZSM-5/Al$_2$O$_3$ extrudates, and desilicated HZSM-5/Al$_2$O$_3$ extrudates. *Energy Fuels* **2019**, *33*, 6405–6420. [CrossRef]

29. Kalogiannis, K.G.; Stefanidis, S.D.; Lappas, A.A. Catalyst deactivation, ash accumulation and bio-oil deoxygenation during ex situ catalytic fast pyrolysis of biomass in a cascade thermal-catalytic reactor system. *Fuel Process. Technol.* **2019**, *186*, 99–109. [CrossRef]

30. Horne, P.A.; Williams, P.T. The effect of zeolite ZSM-5 catalyst deactivation during the upgrading of biomass-derived pyrolysis vapours. *J. Anal. Appl. Pyrolysis* **1995**, *34*, 65–85. [CrossRef]

31. Diebold, J.P.; Scahill, J.W. Biomass To Gasoline (Btg): Upgrading Pyrolysis Vapors To Aromatic Gasoline With Zeolite Catalysis At Atmospheric Pressure. *ACS Div. Fuel Chem. Prepr.* **1987**, *32*, 297–307. [CrossRef]

32. Scahill, J.W.; Diebold, J.P. *Engineering Aspects of Upgrading Pyrolysis oil Using Zeolites*; Elsevier: Amsterdam, The Netherlands, 1988; pp. 927–940.

33. Xu, M.; Mukarakate, C.; Iisa, K.; Budhi, S.; Menart, M.; Davidson, M.; Robichaud, D.J.; Nimlos, M.R.; Trewyn, B.G.; Richards, R.M. *Deactivation of Multilayered MFI Nanosheet Zeolite during Upgrading of Biomass Pyrolysis Vapors*; ACS Publications: Washington, DC, USA, 2017. [CrossRef]

34. Eschenbacher, A.; Andersen, J.A.; Jensen, A.D. Catalytic conversion of acetol over HZSM-5 catalysts—influence of Si/Al ratio and introduction of mesoporosity. *Catal. Today* **2020**. [CrossRef]

35. Eschenbacher, A.; Jensen, P.A.; Henriksen, U.B.; Ahrenfeldt, J.; Ndoni, S.; Li, C.; Duus, J.Ø.; Mentzel, U.V.; Jensen, A.D. Catalytic deoxygenation of vapors obtained from ablative fast pyrolysis of wheat straw using mesoporous HZSM-5. *Fuel Process. Technol.* **2019**, *194*, 106119. [CrossRef]

36. Perkins, G.; Bhaskar, T.; Konarova, M. Process development status of fast pyrolysis technologies for the manufacture of renewable transport fuels from biomass. *Renew. Sustain. Energy Rev.* **2018**, *90*, 292–315. [CrossRef]

37. Menon, P.G. Coke on catalysts-harmful, harmless, invisible and beneficial types. *J. Mol. Catal.* **1990**, *59*, 207–220. [CrossRef]

38. Tamm, P.W.; Harnsberger, H.F.; Bridge, A.G. Effects of Feed Metals on Catalyst Aging in Hydroprocessing Residuum. *Ind. Eng. Chem. Process Des. Dev.* **1981**, *20*, 262–273. [CrossRef]

39. Eschenbacher, A.; Saraeian, A.; Shanks, B.H.; Mentzel, U.V.; Jensen, P.A.; Henriksen, U.B.; Ahrenfeldt, J.; Jensen, A.D. Performance-screening of metal-impregnated industrial HZSM-5/Al$_2$O$_3$ extrudates for deoxygenation and hydrodeoxygenation of fast pyrolysis vapors. *J. Anal. Appl. Pyrolysis.* **2020**, under review.

40. Blasco, T.; Corma, A.; Martínez-Triguero, J. Hydrothermal stabilization of ZSM-5 catalytic-cracking additives by phosphorus addition. *J. Catal.* **2006**, *237*, 267–277. [CrossRef]

41. Huang, L.; Li, Q. Enhanced Acidity and Thermal Stability of Mesoporous Materials with Post-treatment with Phosphoric Acid. *Chem. Lett.* **1999**, *28*, 829–830. [CrossRef]

42. Van der Bij, H.E.; Meirer, F.; Kalirai, S.; Wang, J.; Weckhuysen, B.M. Hexane cracking over steamed phosphated zeolite H-ZSM-5: Promotional effect on catalyst performance and stability. *Chem. A Eur. J.* **2014**, *20*, 16922–16932. [CrossRef]

43. Caeiro, G.; Magnoux, P.; Lopes, J.M.; Ribeiro, F.R.; Menezes, S.M.C.; Costa, A.F.; Cerqueira, H.S. Stabilization effect of phosphorus on steamed H-MFI zeolites. *Appl. Catal. A Gen.* **2006**, *314*, 160–171. [CrossRef]

44. Corma, A.; Mengual, J.; Miguel, P.J. Stabilization of ZSM-5 zeolite catalysts for steam catalytic cracking of naphtha for production of propene and ethene. *Appl. Catal. A Gen.* **2012**, *421–422*, 121–134. [CrossRef]

45. Mante, O.D.; Agblevor, F.A.; Oyama, S.T.; McClung, R. The effect of hydrothermal treatment of FCC catalysts and ZSM-5 additives in catalytic conversion of biomass. *Appl. Catal. A Gen.* **2012**, *445–446*, 312–320. [CrossRef]

46. Yao, W.; Li, J.; Feng, Y.; Wang, W.; Zhang, X.; Chen, Q.; Komarneni, S.; Wang, Y. Thermally stable phosphorus and nickel modified ZSM-5 zeolites for catalytic co-pyrolysis of biomass and plastics. *RSC Adv.* **2015**, *5*, 1–4. [CrossRef]

47. Cerqueira, H.S.; Caeiro, G.; Costa, L.; Ribeiro, F.R. Deactivation of FCC catalysts. *J. Mol. Catal. A Chem.* **2008**, *292*, 1–13. [CrossRef]

48. Van der Bij, H.E.; Weckhuysen, B.M. Local silico-aluminophosphate interfaces within phosphated H-ZSM-5 zeolites. *Phys. Chem. Chem. Phys.* **2014**, *16*, 9892. [CrossRef]

49. Van der Bij, H.E.; Weckhuysen, B.M. Phosphorus promotion and poisoning in zeolite-based materials: Synthesis, characterisation and catalysis. *Chem. Soc. Rev.* **2015**, *44*, 7406–7428. [CrossRef]

50. Bjørgen, M.; Svelle, S.; Joensen, F.; Nerlov, J.; Kolboe, S.; Bonino, F.; Palumbo, L.; Bordiga, S.; Olsbye, U. Conversion of methanol to hydrocarbons over zeolite H-ZSM-5: On the origin of the olefinic species. *J. Catal.* **2007**, *249*, 195–207. [CrossRef]

51. Knöll, J.; Singh, U.; Nicolich, J.; Gonzalez, R.; Ziebarth, M.; Fougret, C.; Brandt, S. Unit cell volume as a measure of dealumination of ZSM-5 in fluid catalytic cracking catalyst. *Ind. Eng. Chem. Res.* **2014**, *53*, 16270–16274. [CrossRef]

52. Degnan, T.F. *Recent Progress in the Development of Zeolitic Catalysts for the Retroleum Refining and Petrochemical Manufacturing Industries*; Elsevier: Amsterdam, The Netherlands, 2007; Volume 170, pp. 54–65. [CrossRef]

53. Gao, X.; Tang, Z.; Ji, D.; Zhang, H. Modification of ZSM-5 zeolite for maximizing propylene in fluid catalytic cracking reaction. *Catal. Commun.* **2009**, *10*, 1787–1790. [CrossRef]

54. Mukarakate, C.; McBrayer, J.D.; Evans, T.J.; Budhi, S.; Robichaud, D.J.; Iisa, K.; Dam, J.t.; Watson, M.J.; Baldwin, R.M.; Nimlos, M.R. Catalytic fast pyrolysis of biomass: The reactions of water and aromatic intermediates produces phenols. *Green Chem.* **2015**, *17*, 4217–4227. [CrossRef]

55. Mullen, C.A.; Tarves, P.C.; Boateng, A.A. Role of Potassium Exchange in Catalytic Pyrolysis of Biomass over ZSM-5: Formation of Alkyl Phenols and Furans. *ACS Sustain. Chem. Eng.* **2017**, *5*, 2154–2162. [CrossRef]

56. Stanton, A.; Iisa, K.; Mukarakate, C.; Nimlos, M.R. Role of Biopolymers in the Deactivation of ZSM-5 during Catalytic Fast Pyrolysis of Biomass. *ACS Sustain. Chem. Eng.* **2018**, *6*, 10030–10038. [CrossRef]

57. Du, S.; Gamliel, D.P.; Valla, J.A.; Bollas, G.M. The effect of ZSM-5 catalyst support in catalytic pyrolysis of biomass and compounds abundant in pyrolysis bio-oils. *J. Anal. Appl. Pyrolysis* **2016**, *122*, 7–12. [CrossRef]

58. Eschenbacher, A.; Goodarzi, F.; Saraeian, A.; Kegnæs, S.; Shanks, B.H.; Jensen, A.D. Performance of Mesoporous HZSM-5 and Silicalite-1 Coated Mesoporous HZSM-5 Catalysts for Deoxygenation of Straw Fast Pyrolysis Vapors. *J. Anal. Appl. Pyrolysis* **2019**, *145*, 104712. [CrossRef]

59. Eschenbacher, A.; Saraeian, A.; Shanks, B.H.; Jensen, P.A.; Henriksen, U.B.; Ahrenfeldt, J.; Jensen, A.D. Insights into the scalability of catalytic upgrading of biomass pyrolysis vapors using micro and bench-scale reactors. *Sustain. Energy Fuels* **2020**, *4*, 3780–3796. [CrossRef]

60. Furimsky, E. Catalytic hydrodeoxygenation. *Appl. Catal. A Gen.* **2000**, *199*, 147–190. [CrossRef]

61. Griffin, M.B.; Iisa, K.; Wang, H.; Dutta, A.; Orton, K.A.; French, R.J.; Santosa, D.M.; Wilson, N.; Christensen, E.; Nash, C.; et al. Driving towards cost-competitive biofuels through catalytic fast pyrolysis by rethinking catalyst selection and reactor configuration. *Energy Environ. Sci.* **2018**, *11*, 2904–2918. [CrossRef]

62. Hoff, T.C.; Thilakaratne, R.; Gardner, D.W.; Brown, R.C.; Tessonnier, J.P. Thermal Stability of Aluminum-Rich ZSM-5 Zeolites and Consequences on Aromatization Reactions. *J. Phys. Chem. C* **2016**, *120*, 20103–20113. [CrossRef]

63. Osman, A.I.; Abu-Dahrieh, J.K.; Rooney, D.W.; Halawy, S.A.; Mohamed, M.A.; Abdelkader, A. Effect of precursor on the performance of alumina for the dehydration of methanol to dimethyl ether. *Appl. Catal. B Environ.* **2012**, *127*, 307–315. [CrossRef]

64. Ong, L.H.; Dömök, M.; Olindo, R.; van Veen, A.C.; Lercher, J.A. Dealumination of HZSM-5 via steam-treatment. *Microporous Mesoporous Mater.* **2012**, *164*, 9–20. [CrossRef]

65. Eschenbacher, A.; Saraeian, A.; Shanks, B.H.; Jensen, P.A.; Li, C.; Duus, Ø. Enhancing bio-oil quality and energy recovery by atmospheric hydrodeoxygenation of wheat straw pyrolysis vapors using Pt and Mo-based catalysts. *Sustain. Energy Fuels* **2020**, *4*, 1991–2008. [CrossRef]

66. Laumer, J.D.S.; Cicchetti, E.; Merle, P.; Egger, J. Quantification in Gas Chromatography Prediction of FID Response Factors from Combustion Enthalpies and Molecular Structures. *Anal. Chem.* **2010**, *82*, 6457–6462. [CrossRef] [PubMed]

67. Chen, N.Y.; Walsh, D.E.; Koenig, L.R. Fluidized Bed Upgrading of Wood Pyrolysis Liquids and Related Compounds. *ACS Div. Fuel Chem. Prepr.* **1987**, *32*, 264–275. [CrossRef]

68. Channiwala, S.A.; Parikh, P.P. A unified correlation for estimating HHV of solid, liquid and gaseous fuels. *Fuel* **2002**, *81*, 1051–1063. [CrossRef]